The Plant Cell, Vol. 32: 2842–2854, September 2020, www.plantcell.org © 2020 ASPB.

Regulation of Female Germline Specification via Small RNA Mobility in Arabidopsis[OPEN]

Zhenxia Su,[a,b,c,d] Nannan Wang,[d] Zhimin Hou,[d] Baiyang Li,[d] Dingning Li,[d] Yanhui Liu,[d] Hanyang Cai,[d] Yuan Qin,[d,e,1] and Xuemei Chen[c,1]

[a] Guangdong Provincial Key Laboratory for Plant Epigenetics, Longhua Institute of Innovative Biotechnology, College of Life Sciences and Oceanography, Shenzhen University, Shenzhen 518060, China
[b] Key Laboratory of Optoelectronic Devices and Systems of Ministry of Education and Guangdong Province, College of Optoelectronic Engineering, Shenzhen University, Shenzhen 518060, China
[c] Department of Botany and Plant Sciences, Institute of Integrative Genome Biology, University of California, Riverside, California 92521
[d] Key Laboratory of Genetics, Breeding, and Multiple Utilization of Crops, Ministry of Education, Fujian Provincial Key Laboratory of Haixia Applied Plant Systems Biology, Fujian Agriculture and Forestry University, Fuzhou 350002, China
[e] State Key Laboratory for Conservation and Utilization of Subtropical Agro-Bioresources, Guangxi Key Laboratory of Sugarcane Biology, College of Agriculture, Guangxi University, Nanning 530004, Guangxi, China

ORCID IDs: 0000-0002-6821-8597 (Z.S.); 0000-0003-3666-1102 (N.W.); 0000-0001-6296-177X (Z.H.); 0000-0002-3961-5972 (B.L.); 0000-0003-0550-0787 (D.L.); 0000-0002-3087-7693 (Y.L.); 0000-0002-6091-888X (H.C.); 0000-0003-4713-6151 (Y.Q.); 0000-0002-5209-1157 (X.C.)

In the ovules of most sexually reproducing plants, one hypodermal cell differentiates into a megaspore mother cell (MMC), which gives rise to the female germline. *Trans*-acting small interfering RNAs known as tasiR-ARFs have been suggested to act non-cell-autonomously to prevent the formation of multiple MMCs by repressing *AUXIN RESPONSE FACTOR3* (*ARF3*) expression in Arabidopsis (*Arabidopsis thaliana*), but the underlying mechanisms are unknown. Here, we examined tasiR-ARF-related intercellular regulatory mechanisms. Expression analysis revealed that components of the tasiR-ARF biogenesis pathway are restricted to distinct ovule cell types, thus limiting tasiR-ARF production to the nucellar epidermis. We also provide data suggesting tasiR-ARF movement along the mediolateral axis into the hypodermal cells and basipetally into the chalaza. Furthermore, we used cell type-specific promoters to express *ARF3m*, which is resistant to tasiR-ARF regulation, in different ovule cell layers. *ARF3m* expression in hypodermal cells surrounding the MMC, but not in epidermal cells, led to a multiple-MMC phenotype, suggesting that tasiR-ARFs repress *ARF3* in these hypodermal cells to suppress ectopic MMC fate. RNA sequencing analyses in plants with hypodermally expressed *ARF3m* showed that *ARF3* potentially regulates MMC specification through phytohormone pathways. Our findings uncover intricate spatial restriction of tasiR-ARF biogenesis, which together with tasiR-ARF mobility enables cell-cell communication in MMC differentiation.

INTRODUCTION

Germline specification is a crucial step in sexual reproduction. Plant reproduction is initiated by the specification of sporocytes that form haploid spores through meiosis. In most sexually reproducing plants, a single somatic, hypodermal cell in the ovule differentiates into a megaspore mother cell (MMC), which gives rise to the female germline (Yang et al., 2010; Grossniklaus, 2011). As the MMC is the first committed cell of the female germline lineage, MMC specification and its regulation are of critical importance.

Trans-acting small interfering RNAs (ta-siRNAs) are a class of endogenous small interfering RNAs (Chen, 2009). The production of ta-siRNAs begins with the transcription of *TAS* loci into long noncoding RNAs by Pol II (Peragine et al., 2004; Vazquez et al., 2004; Yoshikawa et al., 2005). The *TAS* RNAs are exported by the THO/TREX (transcription/export) complex to the cytoplasm (Jauvion et al., 2010; Yelina et al., 2010), where they are targeted for cleavage by ARGONAUTE (AGO) guided by different microRNAs (miR173-AGO1 for *TAS1* and *TAS2*, miR390-AGO7 for *TAS3*, and miR828-AGO1 for *TAS4* in Arabidopsis [*Arabidopsis thaliana*]; Peragine et al., 2004; Vazquez et al., 2004; Allen et al., 2005; Yoshikawa et al., 2005; Rajagopalan et al., 2006; Montgomery et al., 2008a, 2008b; Luo et al., 2012). The cleaved RNA fragments are bound and stabilized by SUPPRESSOR OF GENE SILENCING3 (SGS3) and copied into double-stranded (ds) RNAs by RNA-DEPENDENT RNA POLYMERASE6 (Peragine et al., 2004; Vazquez et al., 2004; Yoshikawa et al., 2005, 2013). DICER-LIKE4 then processes the dsRNAs into phased 21-nucleotide ta-siRNAs from one end of the dsRNAs defined by the cleavage event (Gasciolli et al., 2005; Xie et al., 2005; Yoshikawa et al., 2005). The ta-siRNAs are loaded into the effector AGO1 (Baumberger and Baulcombe, 2005). The tasiR-ARFs from *TAS3* loci are so named because they target several *AUXIN RESPONSE FACTOR* (*ARF*)

[1] Address correspondence to yuanqin@fafu.edu.cn and xuemei.chen@ucr.edu.
The authors responsible for distribution of materials integral to the findings presented in this article in accordance with the policy described in the Instructions for Authors (www.plantcell.org) are: Yuan Qin (yuanqin@fafu.edu.cn) and Xuemei Chen (xuemei.chen@ucr.edu).
[OPEN]Articles can be viewed without a subscription.
www.plantcell.org/cgi/doi/10.1105/tpc.20.00126

genes (Williams et al., 2005; Fahlgren et al., 2006; Garcia et al., 2006; Hunter et al., 2006); they are conserved in angiosperms and play critical roles in plant development (Allen et al., 2005; Nogueira et al., 2007; Marin et al., 2010; Wang et al., 2010; Ozerova et al., 2013; Dotto et al., 2014; Li et al., 2014; Xia et al., 2017).

Recent studies have identified a number of factors involved in MMC differentiation in Arabidopsis (Li et al., 2017; Singh et al., 2017; Cao et al., 2018; Yao et al., 2018). The preferential localization of some of these factors in different ovule cell layers hints at intercellular signaling in MMC specification. We previously showed that *TRANSCRIPTION EXPORT1* (*TEX1*), which encodes a protein in the THO complex involved in the biogenesis of tasiRNAs (Jauvion et al., 2010; Yelina et al., 2010), is specifically expressed in ovule epidermal cells and represses ectopic MMC fate by promoting the biogenesis of tasiR-ARFs. Accordingly, a mutation in *TEX1* leads to the formation of supernumerary MMCs from hypodermal cells (Su et al., 2017). AGO9-dependent 24-nucleotide siRNAs derived from transposable elements were proposed to be produced in epidermal cells and move to the hypodermal, MMC-adjacent cells to prevent them from differentiating into MMCs (Olmedo-Monfil et al., 2010). There may be a similar role for AGO104 during female gametophyte formation in maize (*Zea mays*; Singh et al., 2011). In Arabidopsis, the transcription factor gene *WRKY28* is expressed specifically in the hypodermal somatic cells surrounding the MMC; mutations in *WRKY28* also lead to multiple MMCs in ovule primordia (Zhao et al., 2018). Arabidopsis *MNEME*, a putative RNA helicase gene expressed specifically in the MMC, inhibits neighboring somatic cells from acquiring MMC identity (Schmidt et al., 2011). These findings suggest that intercellular signaling plays key roles in the restriction of the MMC fate to a single cell.

Our previous studies found that *TEX1* represses ectopic MMC fate by spatially restricting the expression of *ARF3* in Arabidopsis ovule primordia. Arabidopsis ovule primordia are radially symmetrical structures with proximal-distal and medial-lateral polarities. Three structural elements, the funiculus, chalaza, and nucellus, can be distinguished along the proximal-distal axis. In wild-type ovules, *ARF3* is expressed in the chalazal region, the central part of the ovule along the proximal-distal axis. However, without proper repression by tasiR-ARFs, *ARF3* is expressed both in the central chalaza and the distal nucellus, including the cells adjacent to the MMC and the outermost epidermal cells (Su et al., 2017). While the ectopic expression of *ARF3* leads to the multiple-MMC phenotype, it is unclear how the tasiR-ARF pathway operates in the ovule to achieve the repression of *ARF3* in MMC-adjacent cells.

In this study, we systematically interrogated the spatial patterns of expression of genes required for tasiR-ARF biogenesis in ovule primordia. We found that *AGO7* expression is concentrated in the nucellar region along the proximal-distal axis and *SGS3* expression is restricted to the epidermis along the medial-lateral axis; the restricted patterns together predict that tasiR-ARF biogenesis occurs in the epidermal layer of the nucellus. We showed that an *ago7* mutant exhibits a multiple-MMC phenotype and that *AGO7* expression in apical, epidermal cells in the mutant was sufficient to rescue the multiple-MMC phenotype. In contrast, AGO1, the protein effector of tasiR-ARFs, exhibited hypodermal cell-enriched localization. Furthermore, we found that the repression of *ARF3* expression in hypodermal cells surrounding the MMC is crucial to ensure the formation of a single MMC. These findings support a mechanism in which tasiR-ARFs produced in the nucellar epidermal cells repress ectopic MMC-like fate by targeting *ARF3* transcripts in the hypodermal cells adjacent to the MMC.

RESULTS

TAS3 Is Transcribed Ubiquitously in Arabidopsis Ovules

To determine the sites of tasiR-ARF biogenesis in ovule primordia, we first investigated the expression patterns of *TAS3* loci, which are transcribed into precursors to tasiR-ARFs, using β-glucuronidase (GUS) reporter constructs driven by the *TAS3A* and *TAS3B* promoters. The constructs were introduced into wild-type Arabidopsis to generate *pTAS3A*:*GUS* and *pTAS3B*:*GUS* stable transformants. Note that *TAS3C* is not expressed at detectable levels in ovules (Su et al., 2017).

GUS histochemical analysis was performed in six to 10 independent T1 transgenic lines for each construct, and typical examples are shown. GUS staining was not detected in control wild-type ovules (Supplemental Figures 1A and 1B). Strong GUS activity was detected in ovules of *pTAS3A*:*GUS* and *pTAS3B*:*GUS* transformants, and the results indicated that *TAS3A* and *TAS3B* have similar, ubiquitous expression patterns during ovule development. At the MMC stage, GUS staining was detected throughout the ovule and in the transmitting tract (Supplemental Figures 1D and 1G), and similar patterns were observed in meiosis-stage ovules (Supplemental Figures 1E and 1H). As the ovules matured, however, GUS activity became weaker (Supplemental Figures 1F and 1I).

MIR390 and *AGO7* Are Involved in MMC Specification

Long noncoding RNAs from the *TAS3* loci are targeted by the miR390-AGO7 complex to trigger tasiR-ARF production (Allen et al., 2005; Montgomery et al., 2008a; Endo et al., 2013). *TAS3A* and *TAS3B* have been shown to regulate MMC specification: the *tas3a* and *tas3b* mutants exhibit a multiple-MMC phenotype in ~20% of ovules (Su et al., 2017). However, it is not known whether *MIR390* or *AGO7* has similar functions in MMC differentiation. We tested this using *mir390* and *ago7* mutants. There are two *MIR390* genes, and the *mir390 52b2* mutant (hereafter referred to as *mir390*) in *MIR390A* has reduced levels of miR390 and tasiR-ARFs (Cuperus et al., 2010). Using differential interference contrast (DIC) observation, the MMC phenotype was analyzed as the frequency of premeiotic ovules with more than one enlarged cell. In *mir390*, ovule primordia containing more than one MMC-like cell occurred at a frequency of 20.2% (Figure 1B), which is higher than that in the wild type (3.2% [$n = 94$]; Figures 1A and 1M) and similar to those of *tas3a* and *tas3b* (Su et al., 2017). For *AGO7*, we examined two mutants, *ago7-9* (SALK_080533) and *zip-2* (Hunter et al., 2006), and the frequencies of ovule primordia with multiple MMC-like cells in these mutants were 24.6 and 22.3%, respectively, which were significantly higher than that in the wild type (Figures 1C, 1D, and 1M). The results above indicated that loss of function in

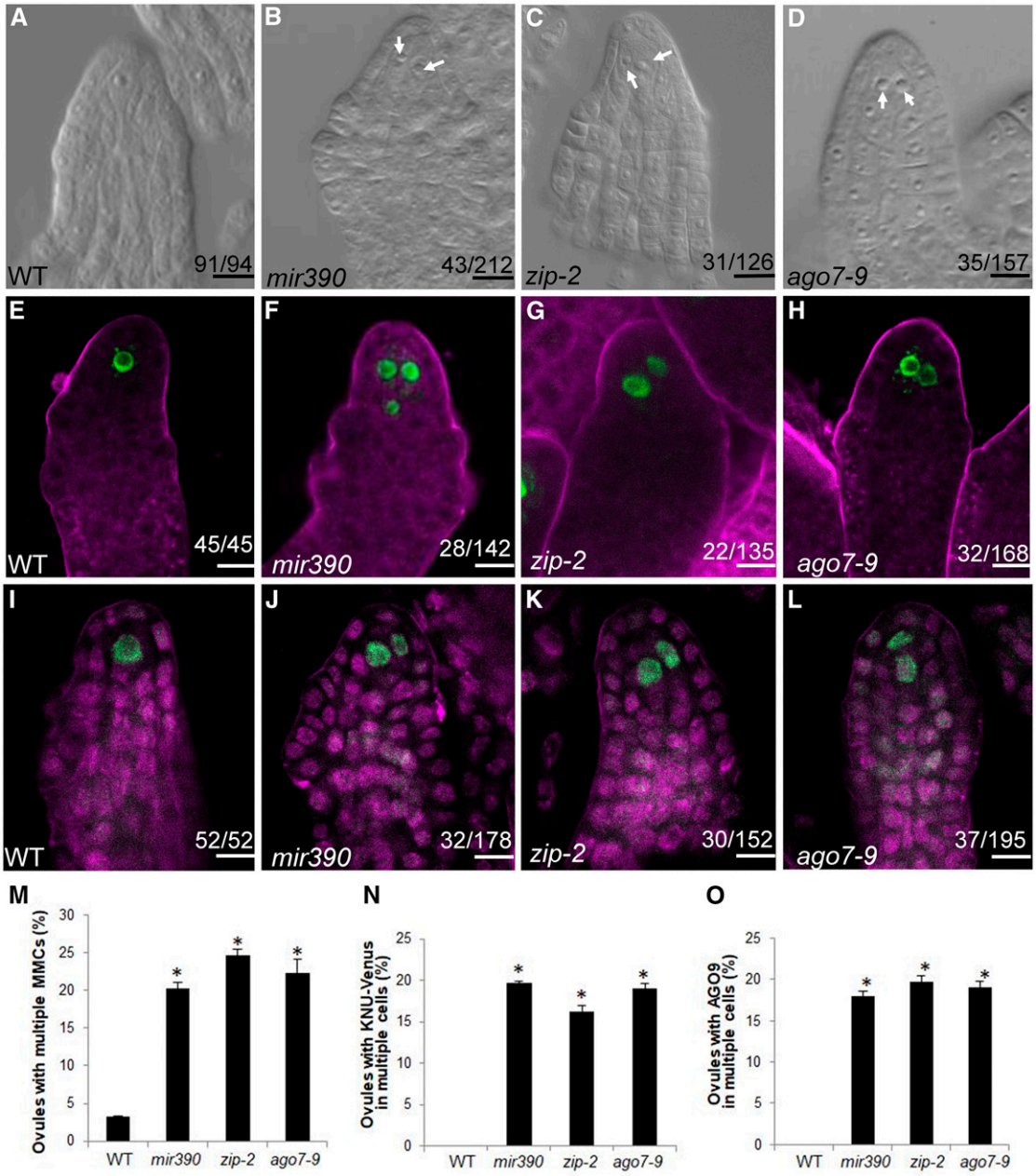

Figure 1. MMC-Like Cells Form in *mir390* and *ago7* Ovules.

(A) Wild-type (WT) ovule with one MMC.
(B) to **(D)** Two MMC-like cells in a *mir390* ovule **(B)**, a *zip-2* ovule **(C)**, and an *ago7-9* ovule **(D)**. MMC-like cells are indicated by white arrows.
(E) Signal corresponding to *pKNU:KNU-Venus* was detected in one cell in wild-type (WT) ovules at the MMC stage. FM4-64 staining is shown in magenta.
(F) to **(H)** Signal corresponding to *pKNU:KNU-Venus* was detected in two or three cells in *mir390* **(F)**, *zip-2* **(G)**, and *ago7-9* **(H)** MMC-stage ovules. FM4-64 staining is shown in magenta.
(I) AGO9 immunolocalization in wild-type (WT) premeiotic ovules. Propidium iodide staining is shown in magenta.
(J) to **(L)** AGO9 immunolocalization in *mir390* **(J)**, *zip-2* **(K)**, and *ago7-9* **(L)** premeiotic ovules. Propidium iodide staining is shown in magenta.
(M) Statistical tests of ovules showing multiple MMCs in the mutants. Significance evaluations between the wild type (WT) and mutants were performed by Student's *t* test (*, $P < 0.05$).
(N) Statistical tests of ovules showing KNU-Venus in multiple cells. Significance evaluations between the wild type (WT) and mutants were performed by Student's *t* test (*, $P < 0.05$).
(O) Statistical tests of ovules showing nuclear AGO9 immunolocalization signal in multiple cells. Significance evaluations between the wild type (WT) and mutants were performed by Student's *t* test (*, $P < 0.05$).
The numbers in each panel indicate the number of ovules with the phenotype shown in the image out of the total number of ovules examined. Bars = 10 μm.

MIR390 and *AGO7* phenocopy *tas3* in having supernumerary MMC-like cells.

To determine whether the supernumerary MMC-like cells in *mir390* and *ago7* had MMC characteristics, we introduced *pKNU*:*KNU-Venus* into *mir390* and *ago7* by crossing. KNU-Venus was detected in the single MMC of wild-type ovule primordia (Figure 1E). In *mir390*, KNU-Venus was observed in more than one cell in 19.7% of ovules. In *zip-2* and *ago7-9*, KNU-Venus was observed in multiple cells in 16.3 and 19.1% of ovules, respectively (Figures 1F to 1H and 1N). The nuclear localization of AGO9 serves as another MMC marker (Figure 1I; Rodríguez-Leal et al., 2015). Whole-mount immunolocalization of AGO9 in these mutants showed that the frequency of premeiotic ovules with AGO9 nuclear localization in multiple MMC-like cells was higher in *mir390*, *zip-2*, and *ago7-9* than in the wild type (Figures 1I to 1L and 1O). Together, the KNU-Venus expression data and the AGO9 localization analysis indicated that the multiple, enlarged MMC-like cells in premeiotic *mir390* and *ago7* ovules acquired MMC characteristics.

To examine whether one or more of the MMC-like cells present in *mir390*, *ago7-9*, and *zip-2* could undergo meiosis, we performed immunolocalization with antibodies against DMC1, which is specifically expressed in the megasporocyte undergoing meiosis in wild-type ovules (Figure 2A; Klimyuk and Jones, 1997; Siddiqi et al., 2000). In *mir390*, *ago7-9*, and *zip-2* ovules, DMC1 signal was only detected in one MMC and not in the other MMC-like cells (Figures 2B to 2D).

In addition to DMC1, we also analyzed callose deposition, another reliable marker for MMCs undergoing meiosis (Webb and Gunning, 1990). In wild-type ovules during meiosis, callose was deposited in the transverse walls between the functional megaspore and its degenerated sister cells (Figures 2E and 2I). In *mir390* postmeiotic ovules, callose was detected in the walls between the single functional megaspore and the degenerated neighboring cells, but it was not detected at the additional, abnormally enlarged cells (Figures 2F and 2J). Similar callose staining results were obtained in the *zip-2* (Figures 2G and 2K) and *ago7-9* (Figures 2H and 2L) mutants.

Based on these findings, we concluded that although multiple MMC-like cells differentiated in *mir390*, *ago7-9*, and *zip-2* ovules, only one underwent meiosis. Thus, the enlarged cells only acquired partial MMC identity. Nevertheless, both *MIR390* and *AGO7* are required to suppress ectopic MMC specification.

miR390 Is Highly Concentrated in the Nucellar Epidermis

Having shown that *MIR390A* is required for the spatial precision in MMC specification, we next studied its expression in ovules using a reporter gene encoding GUS. In *pMIR390A*:*GUS* transformants, strong GUS activity was detected throughout MMC-stage ovules (Figure 3A), indicating that *MIR390A* was transcribed ubiquitously. We then examined miR390 accumulation in ovules by in situ hybridization with an locked nucleic acid (LNA)-modified probe complementary to miR390. In longitudinal sections of ovules, miR390 was present throughout the chalazal region but was concentrated in the epidermis in the nucellar region (Figure 3B). These patterns were further confirmed with cross sections of ovules: signals were nearly absent in the center of the ovule at the base of the nucellar region but were throughout the medial-lateral axis in the chalazal region (Figures 3D and 3E). No signals were detected in wild-type ovules incubated without the probe (Figures 3C and 3F). Thus, despite ubiquitous transcription of *MIR390A* in the ovule, the mature microRNA was at low levels in the MMC and the surrounding cells. This implicated an unknown post-transcriptional mechanism that impacts miR390 accumulation.

AGO7 Is Expressed in the Distal Nucellus of the Ovule

To determine the expression patterns of *AGO7* in ovules, we generated the promoter reporter line *pAGO7*:*GUS* as well as the protein reporter line *pAGO7*:*GFP-AGO7*. Expression analyses were performed with five T1 transgenic plants. In *pAGO7*:*GFP-AGO7* transgenic lines, GFP signal was concentrated in the nucellus, in which cells adjacent to the MMC had particularly strong signals and epidermal cells and the MMC had weaker signals (Figure 3G and 3H). Similar but more strikingly restrictive expression patterns were observed in the promoter reporter line *pAGO7*:*GUS* (Figure 3I).

SGS3 Expression Is Restricted to Epidermal Cells

Following miR390-AGO7-mediated cleavage of *TAS3* transcripts, the cleavage fragments are stabilized by SGS3 in tasiR-ARF biogenesis (Yoshikawa et al., 2005, 2013). It was previously reported that mutations in *SGS3* induce multiple MMCs in Arabidopsis ovule primordia (Olmedo-Monfil et al., 2010). We analyzed *SGS3* expression in ovule primordia using a fusion to GFP or GUS (*pSGS3*:*SGS3-GFP* and *pSGS3*:*SGS3-GUS*). In *pSGS3*:*SGS3-GFP* transgenic lines at the early megasporogenesis stage, SGS3-GFP accumulated specifically in the ovule epidermal cell layer (Figures 3J to 3L). Similar results were obtained in ovules at the later megasporogenesis stage (Supplemental Figures 2A to 2C). The SGS3-GUS expression pattern was also consistent with the SGS3-GFP results (Supplemental Figure 2D). The spatial pattern of *SGS3* expression resembled that of *TEX1* (Su et al., 2017), which is involved in the nuclear export of *TAS3* RNAs in tasiR-ARF biogenesis (Yelina et al., 2010). Thus, the preferential expression of *SGS3* and *TEX1* in the epidermal cell layer of ovule primordia may result in the spatially restricted production of tasiR-ARFs in the ovule.

Apical Epidermal Expression of *AGO7* Is Sufficient to Rescue the MMC Phenotype of *ago7*

The results above show that *AGO7* expression is mainly in the distal nucellus (Figures 3D to 3F) and *SGS3* expression is restricted to the epidermis (Figures 3G to 3I). As both *AGO7* and *SGS3* are required for tasiR-ARF biogenesis, the restricted spatial expression patterns of the two genes probably limit tasiR-ARF biogenesis to the epidermis of the nucellus. If this were the case, we would expect that *AGO7* expression in the epidermis should be sufficient for MMC specification. We expressed *AGO7* with cell layer-specific promoters in the *ago7-9* background to determine where *AGO7* expression is necessary to rescue the multiple-MMC phenotype of *ago7-9*.

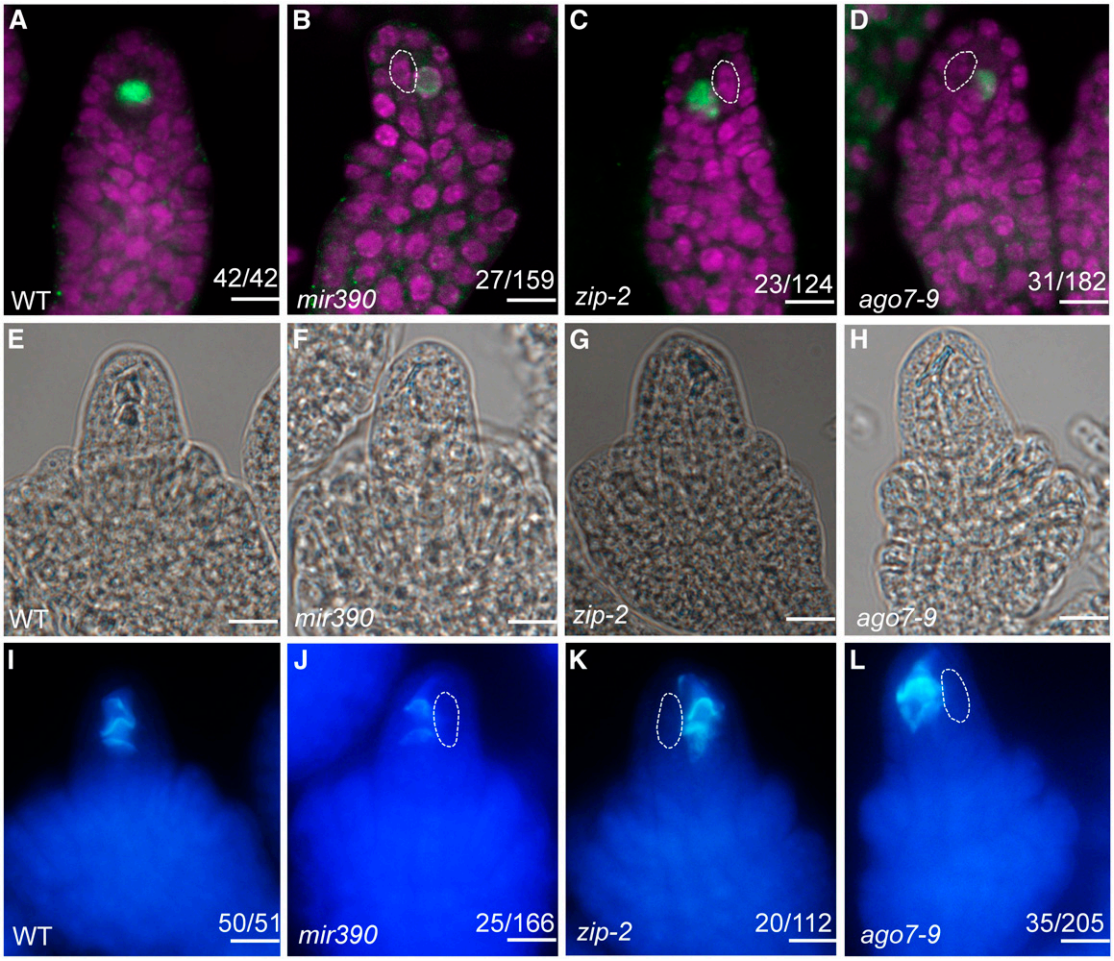

Figure 2. Only One MMC Undergoes Meiosis in *mir390* and *ago7* Ovules.

(A) to **(D)** DMC1 immunolocalization in premeiotic wild-type (WT) **(A)**, *mir390* **(B)**, *zip-2* **(C)**, and *ago7-9* **(D)** ovules. Propidium iodide staining is shown in magenta. Abnormally enlarged cells in **(B)** to **(D)** are outlined with white dashed lines.

(E) to **(L)** Callose deposition in wild-type (WT; **[E]** and **[I]**), *mir390* (**[F]** and **[J]**), *zip-2* (**[G]** and **[K]**), and *ago7-9* (**[H]** and **[L]**) ovules. **(I)** to **(L)** show callose staining with aniline blue, and **(E)** to **(H)** show morphology of the ovules in **(I)** to **(L)**. Abnormally enlarged cells in **(J)** to **(L)** are outlined with white dashed lines. The numbers in each panel indicate the number of ovules with the phenotype shown in the image out of the total number of ovules examined. Bars = 10 μm.

In Arabidopsis, the transcription factor gene *WRKY28* is exclusively expressed in the hypodermal somatic cells surrounding the MMC (Zhao et al., 2018), so we used the *WRKY28* promoter to specifically express *AGO7* in these hypodermal cells (*pWRKY28*:*GFP-AGO7*). Consistent with the *WRKY28* expression pattern, GFP signal was specifically detected in the hypodermal cells surrounding the MMC in *pWRKY28*:*GFP-AGO7 ago7-9* transgenic plants (Figures 4A and 4B). The frequency of premeiotic ovules with more than one MMC-like cell in *pWRKY28*:*GFP-AGO7 ago7-9* lines was 22.5% (n = 182; Figure 4C), comparable to that in *ago7* (Figures 1C and 1D). Thus, expression of *AGO7* in the hypodermal cells surrounding the MMC is unable to rescue the MMC specification defects in *ago7-9*.

SPOROCYTELESS (*SPL*) is required for the differentiation of the megasporocyte and microsporocytes, and it is expressed specifically in the apical epidermal cells at the MMC stage in ovules (Yang et al., 1999; Wei et al., 2015). In *pSPL*:*GFP-AGO7 ago7-9* transgenic plants, the GFP-AGO7 fusion protein was located in the outermost cells of the ovule nucellus (Figures 4D and 4E). Ovules with more than one enlarged cell were detected in these transgenic lines at a low frequency of 4.6% (Figure 4F), comparable to that in the wild type, indicating that *AGO7* expression in the apical epidermal cells could rescue the multiple-MMC phenotype of *ago7-9*. These results also suggested that the production of tasiR-ARFs in apical epidermal cells is critical for MMC differentiation in Arabidopsis.

TasiR-ARFs Repress *ARF3* Expression in Cells Adjacent to the MMC to Prevent Ectopic MMC Differentiation

TasiR-ARFs need to be produced in the epidermal cells of ovule nucellus for correct MMC specification. In which cells do tasiR-ARFs repress *ARF3* expression? To determine the sites of tasiR-ARF function, we analyzed the expression patterns of *ARF3* in

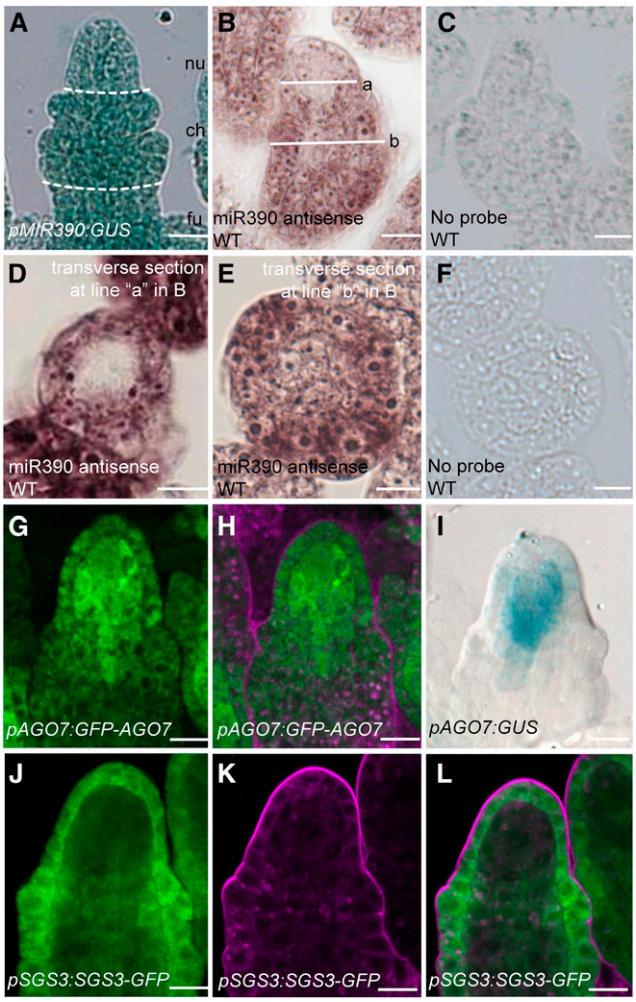

Figure 3. *MIR390*, *AGO7*, and *SGS3* Expression Patterns in Ovules.

(A) GUS signal in a *pMIR390A*:*GUS* ovule. Dashed white lines mark the boundary between the nucellus (nu), chalaza (ch), and funiculus (fu).
(B) In situ localization of miR390 in a longitudinal section through a wild-type (WT) ovule. The white lines represent the positions of transverse sections in **(D)** and **(E)**.
(D) and **(E)** In situ localization of miR390 in transverse sections of nucellus **(D)** and chalaza **(E)** of wild-type (WT) ovules. In **(D)**, the position of the section corresponds to the nucellus region as indicated by line a in **(B)**. In **(E)**, the position of the section corresponds to the chalaza region as indicated by line b in **(B)**.
(C) and **(F)** No signals were detected in longitudinal **(C)** and transverse **(F)** sections of wild-type (WT) ovules incubated without probe.
(G) and **(H)** GFP signal in a *pAGO7*:*GFP-AGO7* ovule. GFP fluorescence is shown in **(G)**; **(H)** shows the same ovule as in **(G)** but with FM4-64 staining.
(I) GUS signal in a *pAGO7*:*GUS* ovule.
(J) to **(L)** GFP signal in a *pSGS3*:*SGS3-GFP* ovule. GFP fluorescence is shown in **(J)**; **(K)** shows the same ovule as in **(J)** but with FM4-64 staining. **(J)** and **(K)** are merged in **(L)**.
Bars = 10 μm.

ovule primordia with or without proper regulation by tasiR-ARFs by whole-mount in situ hybridization. We compared *ARF3* expression between the wild type and the *rdr6-11* mutant, which has greatly reduced levels of tasiR-ARFs (Peragine et al., 2004; Yoshikawa et al., 2005; Su et al., 2017). At the early MMC stage in the wild type, *ARF3* mRNA was detected at the basal end of the chalaza along the proximal-distal axis (Figure 5A). In *rdr6-11*, *ARF3* expression expanded to the apical side of the chalazal region, and weak signals were also detected in the nucellus (Figure 5B). Similar results were observed in late MMC-stage ovules (Figures 5D and 5E). No signals were detected in samples with the *ARF3* sense probe or without probe (Figures 5C and 5F). The in situ hybridization results were consistent with the ARF3-GFP and ARF3m-GFP patterns (resistant to regulation by the tasiR-ARFs) or the ARF3-GFP patterns in *tex1* (defective in the production of tasiR-ARFs) previously reported by Su et al. (2017), with ARF3-GFP mainly in the central chalaza and ARF3m-GFP, as well as ARF3-GFP in *tex1*, in both the central chalaza and distal nucellus. Thus, the activities of tasiR-ARFs exhibited apical polarity in the ovule, with the nucellus and the apical portion of the chalaza being the sites of action.

The above analyses suggest that tasiR-ARFs repress *ARF3* expression in a broad apical domain in ovules, but it is unknown in which cells the repression is necessary for correct MMC specification. To determine whether the development of multiple MMC-like cells was attributable to the expression of *ARF3m* in a specific cell type, we used specific promoters to express *ARF3m* in different ovule cell layers in wild-type plants.

In *pSPL*:*ARF3m-mCitrine* transgenic plants, the ARF3m-mCitrine fusion protein was located in the apical epidermal cells of ovule primordia (Figures 6A to 6C). In *pSPL*:*ARF3m-mCitrine* transgenic lines, the frequency of ovules with more than one

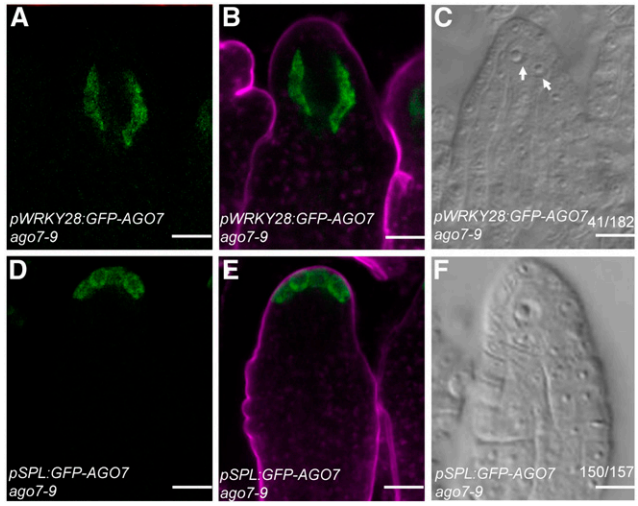

Figure 4. *AGO7* Expression Driven by *pSPL* Rescued the Multiple-MMC Phenotype in *ago7*.

(A) and **(B)** GFP signal in a *pWRKY28*:*GFP-AGO7* ovule. GFP fluorescence is shown in **(A)**; **(B)** shows the same ovule as in **(A)** but with FM4-64 staining.
(C) A *pWRKY28*:*GFP-AGO7* ovule with two MMCs. MMC-like cells are indicated by white arrows.
(D) and **(E)** GFP signal in a *pSPL*:*GFP-AGO7* ovule. GFP fluorescence is shown in **(D)**; **(E)** shows the same ovule as in **(D)** but with FM4-64 staining.
(F) A *pSPL*:*GFP-AGO7* ovule with one MMC.
Bars = 10 μm.

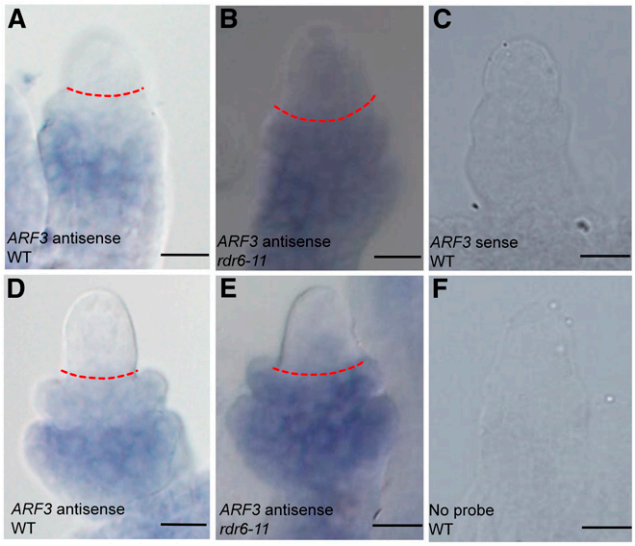

Figure 5. *ARF3* in Situ Hybridization in Ovules.

(A) to **(C)** Whole-mount in situ hybridization of *ARF3* in early MMC-stage wild-type (WT) **(A)** and *rdr6-11* **(B)** ovules. **(C)** shows a wild-type ovule incubated with sense probe.

(D) to **(F)** Whole-mount in situ hybridization of *ARF3* in late MMC-stage wild-type (WT) **(D)** and *rdr6-11* **(H)** ovules. **(F)** shows a WT ovule incubated without probe.

Dashed red lines in **(A)**, **(B)**, **(D)**, and **(E)** mark the boundary between the nucellus and chalaza. Bars = 10 μm.

MMC-like cell was 5.3% (Figure 6D), comparable to that in the wild type, indicating that *ARF3m* expression in the outermost epidermal cells cannot result in multiple enlarged cells in ovule primordia. In *pWRKY28:ARF3m-mCitrine* transgenic lines, mCitrine signal was specifically detected in the hypodermal cells surrounding the MMC (Figures 6E to 6G). DIC observation of the MMC phenotype in *pWRKY28:ARF3m-mCitrine* indicated that premeiotic ovules with more than one enlarged cell occurred at a frequency of 23.5% ($n = 196$; Figure 6H), much higher than that in the wild type and similar to that in *pARF3:ARF3m-GFP* (Su et al., 2017), suggesting that *ARF3m* expression in the hypodermal cells is sufficient to cause the formation of enlarged cells in ovule primordia. For both *pWRKY28:ARF3m-mCitrine* and *pSPL:ARF3m-mCitrine*, RT-qPCR analysis confirmed an increase in *ARF3* transcript levels compared with the wild type (Supplemental Figure 3).

To investigate whether enlarged cells in *pWRKY28:ARF3m-mCitrine* had MMC characteristics, we introduced *pKNU:nls-GUS*, a marker of MMC identity (Payne et al., 2004; Cao et al., 2018) into the transgenic lines by crossing. In wild-type ovule primordia, GUS was detected in the single MMC (Figure 6I). In *pWRKY28:ARF3m-mCitrine*, GUS was observed in two or even three MMC-like cells at a frequency of 20.2%, which was higher than that in the wild type (Figures 6J and 6K). We also performed whole-mount immunolocalization with anti-AGO9 antibodies. In the wild type, AGO9 nuclear localization was detected only in the single MMC (Olmedo-Monfil et al., 2010). In *pWRKY28:ARF3m-mCitrine*, 21.4% of the analyzed ovule primordia had AGO9 nuclear localization in more than one cell (Figure 6L), indicating that the enlarged cells in these transgenic ovule primordia had acquired MMC characteristics. Taken together, these results showed that *ARF3m* expression in the hypodermal cells, but not in the outermost epidermal cells, resulted in multiple MMC-like cells in ovule primordia.

The tasiR-ARFs are recruited into an AGO1-containing effector complex to repress *ARF3* expression (Baumberger and Baulcombe, 2005). In light of the role of AGO1 in mediating the functions of tasiR-ARFs, we investigated the spatial patterns of *AGO1* expression in Arabidopsis ovule primordia using *pAGO1:YFP-AGO1*. At the early megasporogenesis stage, YFP-AGO1 signal was detected in the distal nucellus with preferential expression in hypodermal cells (Supplemental Figures 4A to 4C). This localization pattern was consistent with the finding that the suppression of *ARF3* by tasiR-ARFs occurred in the hypodermal cells surrounding the MMC.

Genes Regulated by *ARF3*

To broaden our investigation of how *ARF3m* expression in ovule hypodermal cells led to the multiple-MMC phenotype, we performed RNA sequencing (RNA-seq) using gynoecia at the MMC stage from wild-type and *pWRKY28:ARF3m-mCitrine* transgenic plants to identify potential downstream genes of *ARF3*. Two replicates were performed and reproducibility was high (Supplemental Figure 5). The analysis identified 447 differentially expressed genes (DEGs; Supplemental Data Set 1), which we considered as candidate target genes regulated by *ARF3*. We compared the publicly available *arf3* mutant gynoecium RNA-seq data (Simonini et al., 2017; Zheng et al., 2018) with our *pWRKY28:ARF3m* RNA-seq data and found only 23 genes in common (Supplemental Data Set 2) between the 447 DEGs in *pWRKY28:ARF3m* versus the wild type and the 738 DEGs in *arf3* versus the wild type, indicating that downstream genes regulated by *ARF3* during MMC differentiation and gynoecium development were largely different.

Gene Ontology (GO) analysis of these 447 DEGs revealed an enrichment of the terms “cellular process” and “metabolic process” (Supplemental Figure 6). Kyoto Encyclopedia of Genes and Genomes pathway enrichment analysis indicated that genes associated with metabolism and plant hormone signal transduction pathways were enriched among the 447 DEGs (Supplemental Figure 7). It has been reported that during the development of ovule primordia, auxin and cytokinin have polarized distributions, with auxin at the distal end and cytokinin at the proximal end (Shirley et al., 2019). Taken together, these results suggest that phytohormones may be involved in MMC differentiation. However, the mechanisms through which hormones exert their functions during this process are still unclear.

DISCUSSION

In this study, we revealed distinct spatial patterns of expression of key components in tasiR-ARF biogenesis in the ovule. From these patterns, it can be deduced that tasiR-ARF production is restricted to the nucellar epidermis. However, the activities of tasiR-ARFs were detected in broader domains, consistent with the mobility of

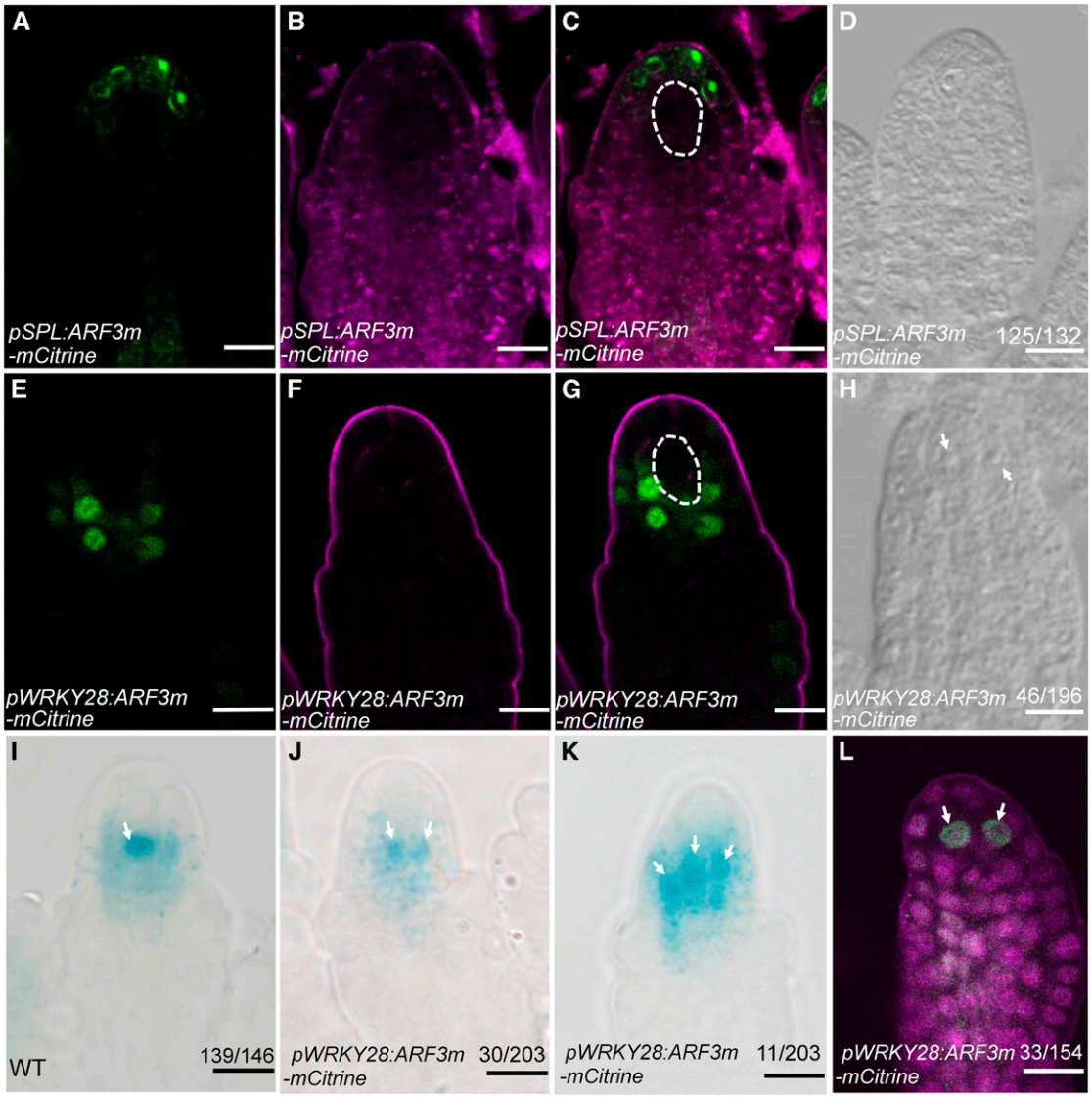

Figure 6. *ARF3m* Expression Driven by *pWRKY28* Resulted in a Multiple-MMC Phenotype.

(A) to **(C)** ARF3m-mCitrine signals in *pSPL:ARF3m-mCitrine* ovules. mCitrine fluorescence is shown in **(A)**. **(A)** and **(B)** are merged in **(C)**. **(B)** shows the same ovules as in **(A)** but with FM4-64 staining. The MMC is marked with white dashed lines in **(C)**.
(D) A *pSPL:ARF3m-mCitrine* ovule with one MMC.
(E) to **(G)** ARF3m-mCitrine signals in *pWRKY28:ARF3m-mCitrine* ovules. mCitrine fluorescence is shown in **(E)**. **(E)** and **(F)** are merged in **(G)**. **(F)** shows the same ovules as in **(E)** but with FM4-64 staining. The MMC is marked with white dashed lines in **(G)**.
(H) A *pWRKY28:ARF3m-mCitrine* ovule with two MMC-like cells. The MMC-like cells are indicated by white arrows.
(I) to **(K)** GUS activity corresponding to *pKNU:nlsGUS* expression in wild-type (WT) **(I)** and *pWRKY28:ARF3m-mCitrine* (**[J]** and **[K]**) ovules. The MMC-like cells are indicated by white arrows.
(L) AGO9 immunolocalization in *pWRKY28:ARF3m-mCitrine* premeiotic ovules. The MMC-like cells are indicated by white arrows.
Bars = 10 μm.

tasiR-ARFs. Furthermore, we found that the expression of *ARF3m*, which is resistant to tasiR-ARF regulation, in the hypodermal cells surrounding the MMC resulted in a multiple-MMC phenotype, suggesting that tasiR-ARFs repress *ARF3* expression in the apical, hypodermal cells to prevent them from adopting an MMC-like fate. This study uncovered extensive coordination between cell layers during MMC specification.

TasiR-ARF Mobility in Arabidopsis Ovule Primordia

TAS3 genes are expressed nearly ubiquitously in ovules, but *SGS3* and *AGO7* have restricted expression patterns in the radial and proximal-distal axes, respectively. *SGS3* is only expressed in the epidermis, and *AGO7* expression is mainly in the distal nucellus. As both *SGS3* and *AGO7* are required for tasiR-ARF

biogenesis, the restricted spatial patterns of the two genes probably limit tasiR-ARF biogenesis to the epidermis of the nucellus. In fact, we demonstrated that the expression of *AGO7* in the distal-most epidermal cells was sufficient to rescue the multiple-MMC phenotype of an *ago7* mutant. The spatial pattern of miR390 accumulation is intriguing: the microRNA is concentrated in the epidermis along the radial axis despite ubiquitous promoter activity. Thus, miR390 is largely excluded from the MMC and its surrounding cells. While it is unknown how this pattern is established, the predominant localization of miR390 in epidermal cells may serve as another piece of evidence for tasiR-ARF biogenesis in the nucellar epidermis.

TasiR-ARFs guide *ARF3* RNA cleavage through their incorporation into an AGO1-containing effector complex (Baumberger and Baulcombe, 2005). The present observation that AGO1 accumulates in the hypodermal cells surrounding the MMC suggests that the cleavage of *ARF3* mRNA by tasiR-ARFs occurs in these cells. This is consistent with the finding that the repression of *ARF3* expression in hypodermal cells is crucial for the suppression of the MMC-like fate.

Previous studies have provided strong evidence that tasiR-ARFs move across cell layers during leaf development. While *TAS3* is transcribed in the epidermal layer to produce the tasiR-ARF precursors, tasiR-ARF abundance follows a gradient emanating from the epidermal layer of leaf primordia (Chitwood et al., 2009). Our study indicates that there may be similar movement of tasiR-ARFs during female gametophyte formation in Arabidopsis. Although our efforts at in situ hybridization to determine the localization of tasiR-ARFs in ovules failed, the expression patterns of different proteins required for tasiR-ARF biogenesis or action suggest the following model. Along the radial axis, tasiR-ARFs are produced in ovule epidermal cells but function in hypodermal cells (Figure 7). Along the proximal-distal axis, tasiR-ARFs are produced in the nucellus but move into the distal chalaza to repress *ARF3* expression (Figure 7).

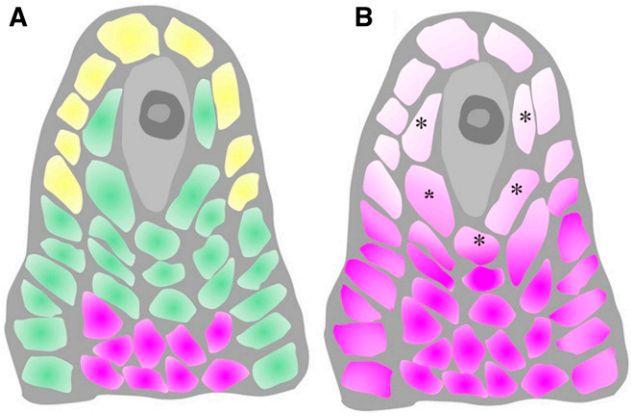

Figure 7. A Model of TasiR-ARF Biogenesis and Mobility.

(A) TasiR-ARFs are processed in the apical epidermal cells (labeled in yellow) and move to hypodermal cells in the nucellar region to restrict *ARF3* expression and suppress MMC identity. The tasiR-ARFs also move basipetally from the nucellus into the chalaza. The distributions of tasiR-ARF3 and *ARF3* RNA are labeled in green and pink, respectively.
(B) Without the control by tasiR-ARFs, *ARF3* expression expands both acropetally and radially. The expression of *ARF3* in the hypodermal cells (labeled with asterisks) leads to MMC characteristics.

Cellular Competence to Acquire MMC Identity in the Hypodermal Cell Layer

In ovules of most sexually reproducing flowering plants, female gametogenesis is initiated from a single gametic cell derived from the MMC (Walbot and Evans, 2003). Because some mutants and certain sexual species develop more than one MMC (Bicknell and Koltunow, 2004; Olmedo-Monfil et al., 2010; Su et al., 2017; Cao et al., 2018; Yao et al., 2018; Zhao et al., 2018) and many species are able to form gametes without meiosis (through apomixis; Bicknell and Koltunow, 2004), it has been proposed that somatic cells in the ovule have the competence to obtain MMC identity.

In Arabidopsis and most angiosperms, the position of the single germline precursor is precisely controlled. Early in ovule development, two layers can be distinguished in the nucellus, the L1 epidermal layer and the L2 hypodermal layer. In Arabidopsis, the distal-most L2 cell becomes the germline MMC. Previous studies have demonstrated that in addition to the distal-most cell, other hypodermal cells have the potential to become MMCs. Olmedo-Monfil et al. (2010) propose that transposable element-derived 24-nucleotide siRNAs produced in epidermal (L1) cells move to the hypodermal nucellar cells to prevent them from differentiating into MMCs. Arabidopsis KLU acts through the chromatin remodeling complex SWR1 to promote *WRKY28* expression specifically in the hypodermal somatic cells surrounding the MMC, and *WRKY28* is required to prevent these cells from acquiring MMC-like characteristics (Zhao et al., 2018). In this study, we found that tasiR-ARFs repress *ARF3* expression in the hypodermal cells to prevent these cells from gaining MMC-like characteristics. To our knowledge, no genes have been reported to be involved in cell identity transitions from epidermal cells to the MMC. In contrast, the derivation of MMC-like cells from hypodermal cells occurs in a number of mutants. This suggests that hypodermal somatic cells have more potential to acquire MMC identity.

Our data showed that the expression of *ARF3* in hypodermal cells adjacent to the MMC promotes the hypodermal cells to gain MMC-like identity, suggesting it is a positive factor for MMC formation. However, its positive effect is limited. In this study, the expression of *ARF3* in the outermost epidermal cells cannot cause the cell fate change from epidermal cell to MMC, suggesting that the expression of *ARF3* is not sufficient for MMC formation. Moreover, in the MMC itself, *ARF3* is not expressed, suggesting that it is not necessary for true MMC fate. These findings implicate the presence of complex regulatory networks in different ovule cell layers and suggest that *ARF3* needs to be repressed in the hypodermal cells surrounding the MMC to prevent these cells from adopting an MMC-like fate.

In summary, this and prior studies show that there are complex regulatory mechanisms that prevent hypodermal cells from gaining MMC identity during ovule development in Arabidopsis. Furthermore, other regulatory factors, such as *SPL* and *WUS*, which promote the formation of the actual MMC, have also been revealed. Mutants of these genes fail to form the actual MMC (Schiefthaler et al., 1999; Yang et al., 1999; Gross-Hardt et al.,

2002). This suggests that dual regulatory mechanisms acting on the MMC and the surrounding cells ensure precise MMC differentiation.

METHODS

Plant Materials and Growth Conditions

Wild-type Arabidopsis (*Arabidopsis thaliana*) Columbia-0 (Col-0), *mir390* (*mir390 52b2*; Cuperus et al., 2010), *ago7-9* (SALK_080533), *MIR390:GUS* (CS66476), and *zip-2* (CS24282; Hunter et al., 2006) were grown under 16-h-light (50 μmol m^{-2} s^{-1}, white light)/8-h-dark conditions at 22°C.

Plasmid Construction

For the *pTAS3A*:*GUS* and *pTAS3B*:*GUS* plasmids, a 2150-bp sequence upstream of *TAS3A* and a 1463-bp sequence upstream of *TAS3B* were amplified from wild-type genomic DNA using primers listed in the Supplemental Table. The PCR fragments were cloned into the pENTR/D-TOPO (Invitrogen) vector and verified by sequencing. The fragments were subsequently recombined into the destination vector pMDC162 (Curtis and Grossniklaus, 2003) using LR Clonase II (Invitrogen).

For *pSPL*:*ARF3m-mCitrine*, a 2704-bp sequence upstream of *SPL* was amplified as the promoter *pSPL* from wild-type genomic DNA using the primers pSPL-F and pSPL-R (Supplemental Table). The *ARF3m* fragment was amplified from the *pARF3*:*ARF3m-GFP* plasmid (Liu et al., 2014) using primers ARF3m-F and ARF3m-R (Supplemental Table). The *pSPL*:*ARF3m* fragment was generated by PCR using a mixture of *pSPL* and *ARF3m* as the template and cloned into the pENTR/D-TOPO (Invitrogen) vector. The presence of the tasiR-ARF-resistant mutation in *pSPL-ARF3m* was verified by sequencing. Finally, recombination into the destination vector pGWB5012 (Nakagawa et al., 2007) was performed using LR Clonase II to generate *pSPL*:*ARF3m-mCitrine*. For *pWRKY28*:*ARF3m-mCitrine*, a 2097-bp sequence upstream of *WRKY28* was amplified using the primers *pWRKY28-F* and *pWRKY28-R* (Supplemental Table). The subsequent steps to construct *pWRKY28*:*ARF3m-mCitrine* were as described above for *pSPL*:*ARF3m-mCitrine*.

For *pAGO7*:*GUS*, a 2081-bp sequence upstream of *AGO7* was amplified as the promoter *pAGO7* using primers pAGO7-F and pAGO7-R (Supplemental Table). The PCR fragment was cloned into pENTR/D-TOPO (Invitrogen) and verified by DNA sequencing, followed by recombination into the destination vector pGWB533 (Nakagawa et al., 2007) using LR Clonase II.

To generate the *pAGO7*:*GFP-AGO7*, *pSPL*:*GFP-AGO7*, and *pWRKY28*:*GFP-AGO7* constructs, the *pAGO7*, *pSPL*, and *pWRKY28* promoters were amplified from Arabidopsis genomic DNA as described above, and the *GFP* fragment was amplified from pGWB504 (Nakagawa et al., 2007). The *AGO7* sequence was amplified by PCR using Arabidopsis cDNA as the template using primers AGO7cds-F and AGO7cds-R (Supplemental Table). *pAGO7*:*GFP-AGO7*, *pSPL*:*GFP-AGO7*, and *pWRKY28*:*GFP-AGO7* were cloned into pENTR/D-TOPO (Invitrogen) by infusion, followed by recombination into the destination vector pGWB501 (Nakagawa et al., 2007) using LR Clonase II.

To construct *pSGS3*:*SGS3-GFP* and *pSGS3*:*SGS3-GUS*, a genomic fragment encompassing 2148 bp upstream of the start codon of *SGS3* and a 2251-bp *SGS3* coding region without the stop codon was amplified with primers pSGS3-F and SGS3-R. The PCR product was cloned into pENTR/D-TOPO (Invitrogen) and verified by sequencing. The fragment was recombined by LR reaction into the destination vectors pGWB504 (Nakagawa et al., 2007) and pGWB533 (Nakagawa et al., 2007) to obtain *pSGS3*:*SGS3-GFP* and *pSGS3*:*SGS3-GUS*, respectively.

Preparation of Ovules for Confocal Laser Scanning Microscopy

Ovules were dissected, stained in 40% (v/v) glycerol with 5 mM FM4-64 for 5 min, and then analyzed using a TCS SP8 microscope (Leica). For the expression pattern analysis of the transgenic lines, more than five independent transgenic lines were observed and confirmed to have similar patterns.

Real-Time qPCR

To measure the relative transcript levels of selected genes, real-time qPCR was performed with specific primers (Supplemental Table) using the Bio-Rad real-time PCR system and SYBR Premix Ex Taq II (TaKaRa) according to the manufacturer's instructions.

DIC Observation of Ovule Structures

Ovules from wild-type, mutant, and transgenic plants were dissected from the pistils of stages 8 to 13 flowers (Robinson-Beers et al., 1992) in a drop of chloral hydrate solution (chloral hydrate:water:glycerol = 8:1:3 [m/v/v]). A BX63 microscope with DIC optics (Olympus) was used to obtain images of the cleared ovules with a 40× objective.

GUS Staining

Inflorescence samples were fixed in prechilled 80% (v/v) acetone for 20 min and then washed with distilled water. After brief vacuum infiltration, the inflorescences were incubated in GUS staining buffer (Oh et al., 2010) overnight at 37°C. The pistils were dissected from the inflorescences and then observed with a BX63 microscope (Olympus).

Whole-Mount Immunolocalization in Ovules

Ovules were dissected from 30 to 40 pistils of stage 9 to 11 flowers (Robinson-Beers et al., 1992) and then fixed and processed according to a protocol previously published by Escobar-Guzmán et al. (2015). The AGO9 primary antibody (Agrisera AS10673) and DMC1 primary antibody (ABclonal Technology) were used at a dilution of 1:100. The Alexa Fluor 488 secondary antibody (Molecular Probes) was used at a dilution of 1:300. The samples were stained with propidium iodide (500 mg/mL) before mounting, and images were captured using a confocal microscope (Leica TCS SP8). For propidium iodide detection, the excitation and emission wavelengths were 568 nm and 575 to 615 nm, respectively. For Alexa Fluor 488 detection, the excitation and emission wavelengths were 488 nm and 500 to 550 nm, respectively. The laser intensity and gain were set to the same levels for all analyzed genotypes.

ARF3 Whole-Mount in Situ Hybridization in Ovules

Ovules with placenta were dissected from pistils of stage 9 to 11 flowers and then fixed and processed as previously described by Zhao et al. (2018). For the *ARF3* probe, a 209-bp cDNA fragment was amplified by PCR with primers ARF3-IS-F and ARF3-IS-R (Supplemental Table) and cloned into the pTA2 vector (Toyobo). Generation of digoxigenin-labeled probe was performed as described by Sieber et al. (2004). Ovule whole-mount in situ hybridization was performed according to Hejátko et al. (2006).

miR390 in Situ Hybridization for Paraffin-Embedded Ovules

The sequence of the LNA probe to detect mature miR390 is GGCGCU A+UC+CC+UCC+UGAGCUU (GenScript), in which + represents the LNA position. Developing floral buds at the MMC stage were fixed and embedded in Paraplast Plus embedding medium, cut into 6-μm sections,

and then hybridized to the probe as previously described by Kidner and Timmermans (2006).

Callose Detection

Aniline blue staining and callose detection in the megaspores were performed as previously described by Siddiqi et al. (2000) with minor modifications, including fixation of inflorescences in formaldehyde/ alcohol/ acetic acid for 16 h and incubation in 0.1% (w/v) aniline blue in 50 mM phosphate buffer (pH 11) for 8 to 12 h. The stained pistils were mounted in 30% (v/v) glycerol and observed with a BX63 microscope (Olympus) at an excitation wavelength of 365 nm and using an emission long-pass filter of 420 nm.

RNA-Seq and Data Analysis

RNA was extracted from gynoecia at the MMC stage (Robinson-Beers et al., 1992) from wild-type and *pWRKY28:ARF3m-mCitrine* plants using the Qiagen RNeasy kit. Illumina sequencing was performed using 1 μg of RNA per sample and two independent biological replicates per genotype. The raw reads were filtered by removing the adapter sequences and low-quality reads. Using the The Arabidopsis Information Resource 10 assembly as the reference genome, the clean reads were aligned using STAR v2.5.0, and the alignment results were processed using the SourceForge Subread package featureCount v1.5.0 for RNA quantification. EdgeR v3.12.0 was used to identify differentially expressed genes (fold change ≥ 2, false discovery rate ≤ 0.05) between samples.

GO and Pathway Enrichment Analyses

GO enrichment analysis for differentially expressed gene sets was performed using TBtools (Chen et al., 2018). The P value for enrichment was calculated for each represented GO term and corrected via the Benjamini-Hochberg error correction method (Ferreira and Nyangoma, 2008). The GO terms exhibiting a corrected $P \leq 0.05$ were considered to be significantly enriched. Furthermore, pathway enrichment analysis of different sets of genes was also performed using TBtools.

Accession Numbers

Sequence data from this article can be found in the Arabidopsis Genome Initiative or GenBank/EMBL databases under the following accession numbers: *TAS3A* (AT3G17185), *TAS3B* (AT5G49615), *ARF3* (AT2G33860), *WRKY28* (AT4G18170), *SPL* (AT4G27330), *AGO7* (AT1G69440), *MIR390A* (AT2G38325), *SGS3* (AT5G23570), and *AGO1* (AT1G48410). The RNA-seq data were deposited in the European Nucleotide Archive under accession number PRJEB38604.

Supplemental Data

Supplemental Figure 1. *pTAS3:GUS* expression in Arabidopsis ovules.

Supplemental Figure 2. *SGS3* expression in later MMC stage Arabidopsis ovules.

Supplemental Figure 3. *ARF3* transcript levels in the wild type and the transgenic lines *pSPL:ARF3m-mCitrine* and *pWRKY28:ARF3m-mCitrine*.

Supplemental Figure 4. *AGO1* expression in Arabidopsis MMC-stage ovules.

Supplemental Figure 5. The consistency of RNA-seq replicates for the wild type and *pWRKY28:ARF3m-mCitrine*.

Supplemental Figure 6. GO analysis of DEGs in *pWRKY28:ARF3m-mCitrine* compared with the wild type.

Supplemental Figure 7. Kyoto Encyclopedia of Genes and Genomes pathway enrichment analysis of DEGs in *pWRKY28:ARF3m-mCitrine* compared with the wild type.

Supplemental Table. Primers and probes used in this study.

Supplemental Data Set 1. The DEGs of *pWRKY28:ARF3m-mCitrine* compared with the wild type.

Supplemental Data Set 2. The DEGs in common between *pWRKY28:ARF3m* versus the wild type and *arf3* versus the wild type.

AUTHOR CONTRIBUTIONS

Z.S., Y.Q., and X.C. conceived the project; Z.S., N.W., and Z.H. designed and performed the experiments; B.L., D.L., Y.L., and H.C. analyzed the data; Z.S., Y.Q., and X.C. wrote the article.

We thank Xigang Liu (Institute of Genetics and Developmental Biology, Chinese Academy of Sciences) for the kind gift of the *ARF3:ARF3m-GFP* plasmid and Hong Wang (Department of Biochemistry, University of Saskatchewan) for sharing the *pKNU:nlsGUS* plasmid. This work was supported by the Guangdong Innovation Research Team Fund (grant 2014ZT05S078 to Z.S.), the National Natural Science Foundation of China (grant 31700278 to Z.S. and grants 31970333 and 31761130074 to Y.Q.), the China Postdoctoral Science Foundation (grant 2018T110888 to Z.S.), the Guangxi Distinguished Experts Fellowship and a Newton Advanced Fellowship (grant NA160391 to Y.Q.), and the NIH (grant GM129373 to X.C.).

Received February 18, 2020; revised June 30, 2020; accepted July 23, 2020; published July 23, 2020.

REFERENCES

Allen, E., Xie, Z., Gustafson, A.M., and Carrington, J.C. (2005). MicroRNA-directed phasing during trans-acting siRNA biogenesis in plants. Cell **121:** 207–221.

Baumberger, N., and Baulcombe, D.C. (2005). Arabidopsis ARGONAUTE1 is an RNA Slicer that selectively recruits microRNAs and short interfering RNAs. Proc. Natl. Acad. Sci. USA **102:** 11928–11933.

Bicknell, R.A., and Koltunow, A.M. (2004). Understanding apomixis: Recent advances and remaining conundrums. Plant Cell **16** (suppl.): S228–S245.

Cao, L., Wang, S., Venglat, P., Zhao, L., Cheng, Y., Ye, S., Qin, Y., Datla, R., Zhou, Y., and Wang, H. (2018). Arabidopsis ICK/KRP cyclin-dependent kinase inhibitors function to ensure the formation of one megaspore mother cell and one functional megaspore per ovule. PLoS Genet. **14:** e1007230.

Chen, C., Xia, R., Chen, H., and He, Y.J.B. (2018). TBtools, a toolkit for biologists integrating various biological data handling tools with a user-friendly interface. bioRxiv. Available at: https://doi.org/10.1101/289660.

Chen, X. (2009). Small RNAs and their roles in plant development. Annu. Rev. Cell Dev. Biol. **25:** 21–44.

Chitwood, D.H., Nogueira, F.T., Howell, M.D., Montgomery, T.A., Carrington, J.C., and Timmermans, M.C. (2009). Pattern formation via small RNA mobility. Genes Dev. **23:** 549–554.

Cuperus, J.T., Montgomery, T.A., Fahlgren, N., Burke, R.T., Townsend, T., Sullivan, C.M., and Carrington, J.C. (2010). Identification of MIR390a precursor processing-defective mutants in Arabidopsis by direct genome sequencing. Proc. Natl. Acad. Sci. USA **107:** 466–471.

Curtis, M.D., and Grossniklaus, U. (2003). A gateway cloning vector set for high-throughput functional analysis of genes in planta. Plant Physiol. **133:** 462–469.

Dotto, M.C., Petsch, K.A., Aukerman, M.J., Beatty, M., Hammell, M., and Timmermans, M.C. (2014). Genome-wide analysis of leafbladeless1-regulated and phased small RNAs underscores the importance of the TAS3 ta-siRNA pathway to maize development. PLoS Genet. **10:** e1004826.

Endo, Y., Iwakawa, H.O., and Tomari, Y. (2013). Arabidopsis ARGONAUTE7 selects miR390 through multiple checkpoints during RISC assembly. EMBO Rep. **14:** 652–658.

Escobar-Guzmán, R., Rodríguez-Leal, D., Vielle-Calzada, J.P., and Ronceret, A. (2015). Whole-mount immunolocalization to study female meiosis in Arabidopsis. Nat. Protoc. **10:** 1535–1542.

Fahlgren, N., Montgomery, T.A., Howell, M.D., Allen, E., Dvorak, S.K., Alexander, A.L., and Carrington, J.C. (2006). Regulation of AUXIN RESPONSE FACTOR3 by TAS3 ta-siRNA affects developmental timing and patterning in Arabidopsis. Curr. Biol. **16:** 939–944.

Ferreira, J.A., and Nyangoma, S.O. (2008). A multivariate version of the Benjamini-Hochberg method. J. Multivariate Anal. **99:** 2108–2124.

Garcia, D., Collier, S.A., Byrne, M.E., and Martienssen, R.A. (2006). Specification of leaf polarity in Arabidopsis via the trans-acting siRNA pathway. Curr. Biol. **16:** 933–938.

Gasciolli, V., Mallory, A.C., Bartel, D.P., and Vaucheret, H. (2005). Partially redundant functions of Arabidopsis DICER-like enzymes and a role for DCL4 in producing trans-acting siRNAs. Curr. Biol. **15:** 1494–1500.

Gross-Hardt, R., Lenhard, M., and Laux, T. (2002). WUSCHEL signaling functions in interregional communication during Arabidopsis ovule development. Genes Dev. **16:** 1129–1138.

Grossniklaus, U. (2011). Plant germline development: A tale of cross-talk, signaling, and cellular interactions. Sex. Plant Reprod. **24:** 91–95.

Hejátko, J., Blilou, I., Brewer, P.B., Friml, J., Scheres, B., and Benková, E. (2006). In situ hybridization technique for mRNA detection in whole mount Arabidopsis samples. Nat. Protoc. **1:** 1939–1946.

Hunter, C., Willmann, M.R., Wu, G., Yoshikawa, M., de la Luz Gutiérrez-Nava, M., and Poethig, S.R. (2006). Trans-acting siRNA-mediated repression of ETTIN and ARF4 regulates heteroblasty in Arabidopsis. Development **133:** 2973–2981.

Jauvion, V., Elmayan, T., and Vaucheret, H. (2010). The conserved RNA trafficking proteins HPR1 and TEX1 are involved in the production of endogenous and exogenous small interfering RNA in Arabidopsis. Plant Cell **22:** 2697–2709.

Kidner, C., and Timmermans, M. (2006). In situ hybridization as a tool to study the role of microRNAs in plant development. Methods Mol. Biol. **342:** 159–179.

Klimyuk, V.I., and Jones, J.D. (1997). AtDMC1, the Arabidopsis homologue of the yeast DMC1 gene: Characterization, transposon-induced allelic variation and meiosis-associated expression. Plant J. **11:** 1–14.

Li, L., Wu, W., Zhao, Y., and Zheng, B. (2017). A reciprocal inhibition between ARID1 and MET1 in male and female gametes in Arabidopsis. J. Integr. Plant Biol. **59:** 657–668.

Li, X., Lei, M., Yan, Z., Wang, Q., Chen, A., Sun, J., Luo, D., and Wang, Y. (2014). The REL3-mediated TAS3 ta-siRNA pathway integrates auxin and ethylene signaling to regulate nodulation in *Lotus japonicus*. New Phytol. **201:** 531–544.

Liu, X., Dinh, T.T., Li, D., Shi, B., Li, Y., Cao, X., Guo, L., Pan, Y., Jiao, Y., and Chen, X. (2014). AUXIN RESPONSE FACTOR 3 integrates the functions of AGAMOUS and APETALA2 in floral meristem determinacy. Plant J. **80:** 629–641.

Luo, Q.J., Mittal, A., Jia, F., and Rock, C.D. (2012). An autoregulatory feedback loop involving PAP1 and TAS4 in response to sugars in Arabidopsis. Plant Mol. Biol. **80:** 117–129.

Marin, E., Jouannet, V., Herz, A., Lokerse, A.S., Weijers, D., Vaucheret, H., Nussaume, L., Crespi, M.D., and Maizel, A. (2010). miR390, Arabidopsis TAS3 tasiRNAs, and their AUXIN RESPONSE FACTOR targets define an autoregulatory network quantitatively regulating lateral root growth. Plant Cell **22:** 1104–1117.

Montgomery, T.A., Howell, M.D., Cuperus, J.T., Li, D., Hansen, J.E., Alexander, A.L., Chapman, E.J., Fahlgren, N., Allen, E., and Carrington, J.C. (2008a). Specificity of ARGONAUTE7-miR390 interaction and dual functionality in TAS3 trans-acting siRNA formation. Cell **133:** 128–141.

Montgomery, T.A., Yoo, S.J., Fahlgren, N., Gilbert, S.D., Howell, M.D., Sullivan, C.M., Alexander, A., Nguyen, G., Allen, E., Ahn, J.H., and Carrington, J.C. (2008b). AGO1-miR173 complex initiates phased siRNA formation in plants. Proc. Natl. Acad. Sci. USA **105:** 20055–20062.

Nakagawa, T., Kurose, T., Hino, T., Tanaka, K., Kawamukai, M., Niwa, Y., Toyooka, K., Matsuoka, K., Jinbo, T., and Kimura, T. (2007). Development of series of gateway binary vectors, pGWBs, for realizing efficient construction of fusion genes for plant transformation. J. Biosci. Bioeng. **104:** 34–41.

Nogueira, F.T., Madi, S., Chitwood, D.H., Juarez, M.T., and Timmermans, M.C. (2007). Two small regulatory RNAs establish opposing fates of a developmental axis. Genes Dev. **21:** 750–755.

Oh, S.A., Pal, M.D., Park, S.K., Johnson, J.A., and Twell, D. (2010). The tobacco MAP215/Dis1-family protein TMBP200 is required for the functional organization of microtubule arrays during male germline establishment. J. Exp. Bot. **61:** 969–981.

Olmedo-Monfil, V., Durán-Figueroa, N., Arteaga-Vázquez, M., Demesa-Arévalo, E., Autran, D., Grimanelli, D., Slotkin, R.K., Martienssen, R.A., and Vielle-Calzada, J.P. (2010). Control of female gamete formation by a small RNA pathway in Arabidopsis. Nature **464:** 628–632.

Ozerova, L.V., Krasnikova, M.S., Troitsky, A.V., Solovyev, A.G., and Morozov, S.Y. (2013). TAS3 genes for small ta-siARF RNAs in plants belonging to subtribe Senecioninae: Occurrence of prematurely terminated RNA precursors. Mol. Gen. Mikrobiol. Virusol. 33–36.

Payne, T., Johnson, S.D., and Koltunow, A.M. (2004). KNUCKLES (KNU) encodes a C2H2 zinc-finger protein that regulates development of basal pattern elements of the Arabidopsis gynoecium. Development **131:** 3737–3749.

Peragine, A., Yoshikawa, M., Wu, G., Albrecht, H.L., and Poethig, R.S. (2004). SGS3 and SGS2/SDE1/RDR6 are required for juvenile development and the production of trans-acting siRNAs in Arabidopsis. Genes Dev. **18:** 2368–2379.

Rajagopalan, R., Vaucheret, H., Trejo, J., and Bartel, D.P. (2006). A diverse and evolutionarily fluid set of microRNAs in Arabidopsis thaliana. Genes Dev. **20:** 3407–3425.

Robinson-Beers, K., Pruitt, R.E., and Gasser, C.S. (1992). Ovule development in wild-type Arabidopsis and two female-sterile mutants. Plant Cell **4:** 1237–1249.

Rodríguez-Leal, D., León-Martínez, G., Abad-Vivero, U., and Vielle-Calzada, J.P. (2015). Natural variation in epigenetic pathways affects the specification of female gamete precursors in Arabidopsis. Plant Cell **27:** 1034–1045.

Schiefthaler, U., Balasubramanian, S., Sieber, P., Chevalier, D., Wisman, E., and Schneitz, K. (1999). Molecular analysis of NOZZLE, a gene involved in pattern formation and early sporogenesis during sex organ development in *Arabidopsis thaliana*. Proc. Natl. Acad. Sci. USA **96:** 11664–11669.

Schmidt, A., Wuest, S.E., Vijverberg, K., Baroux, C., Kleen, D., and Grossniklaus, U. (2011). Transcriptome analysis of the Arabidopsis megaspore mother cell uncovers the importance of RNA helicases for plant germline development. PLoS Biol. **9:** e1001155.

Shirley, N.J., Aubert, M.K., Wilkinson, L.G., Bird, D.C., Lora, J., Yang, X., and Tucker, M.R. (2019). Translating auxin responses into ovules, seeds and yield: Insight from Arabidopsis and the cereals. J. Integr. Plant Biol. **61:** 310–336.

Siddiqi, I., Ganesh, G., Grossniklaus, U., and Subbiah, V. (2000). The dyad gene is required for progression through female meiosis in Arabidopsis. Development **127:** 197–207.

Sieber, P., Gheyselinck, J., Gross-Hardt, R., Laux, T., Grossniklaus, U., and Schneitz, K. (2004). Pattern formation during early ovule development in *Arabidopsis thaliana*. Dev. Biol. **273:** 321–334.

Simonini, S., Bencivenga, S., Trick, M., and Østergaard, L. (2017). Auxin-induced modulation of ETTIN activity orchestrates gene expression in Arabidopsis. Plant Cell **29:** 1864–1882.

Singh, M., Goel, S., Meeley, R.B., Dantec, C., Parrinello, H., Michaud, C., Leblanc, O., and Grimanelli, D. (2011). Production of viable gametes without meiosis in maize deficient for an ARGONAUTE protein. Plant Cell **23:** 443–458.

Singh, S.K., Kumar, V., Srinivasan, R., Ahuja, P.S., Bhat, S.R., and Sreenivasulu, Y. (2017). The *TRAF Mediated Gametogenesis Progression* (*TRAMGaP*) gene is required for megaspore mother cell specification and gametophyte development. Plant Physiol. **175:** 1220–1237.

Su, Z., et al. (2017). The THO complex non-cell-autonomously represses female germline specification through the TAS3-ARF3 module. Curr. Biol. **27:** 1597–1609.e1592.

Vazquez, F., Vaucheret, H., Rajagopalan, R., Lepers, C., Gasciolli, V., Mallory, A.C., Hilbert, J.L., Bartel, D.P., and Crété, P. (2004). Endogenous trans-acting siRNAs regulate the accumulation of Arabidopsis mRNAs. Mol. Cell **16:** 69–79.

Walbot, V., and Evans, M.M. (2003). Unique features of the plant life cycle and their consequences. Nat. Rev. Genet. **4:** 369–379.

Wang, J., Gao, X., Li, L., Shi, X., Zhang, J., and Shi, Z. (2010). Overexpression of Osta-siR2141 caused abnormal polarity establishment and retarded growth in rice. J. Exp. Bot. **61:** 1885–1895.

Webb, M.C., and Gunning, B.E.S. (1990). Embryo sac development in *Arabidopsis thaliana*. Sex. Plant Reprod. **3:** 13.

Wei, B., Zhang, J., Pang, C., Yu, H., Guo, D., Jiang, H., Ding, M., Chen, Z., Tao, Q., Gu, H., Qu, L.J., and Qin, G. (2015). The molecular mechanism of sporocyteless/nozzle in controlling Arabidopsis ovule development. Cell Res. **25:** 121–134.

Williams, L., Carles, C.C., Osmont, K.S., and Fletcher, J.C. (2005). A database analysis method identifies an endogenous trans-acting short-interfering RNA that targets the Arabidopsis ARF2, ARF3, and ARF4 genes. Proc. Natl. Acad. Sci. USA **102:** 9703–9708.

Xia, R., Xu, J., and Meyers, B.C. (2017). The emergence, evolution, and diversification of the miR390-*TAS3*-*ARF* pathway in land plants. Plant Cell **29:** 1232–1247.

Xie, Z., Allen, E., Wilken, A., and Carrington, J.C. (2005). DICER-LIKE 4 functions in trans-acting small interfering RNA biogenesis and vegetative phase change in *Arabidopsis thaliana*. Proc. Natl. Acad. Sci. USA **102:** 12984–12989.

Yang, W.C., Shi, D.Q., and Chen, Y.H. (2010). Female gametophyte development in flowering plants. Annu. Rev. Plant Biol. **61:** 89–108.

Yang, W.C., Ye, D., Xu, J., and Sundaresan, V. (1999). The SPOROCYTELESS gene of Arabidopsis is required for initiation of sporogenesis and encodes a novel nuclear protein. Genes Dev. **13:** 2108–2117.

Yao, X., Yang, H., Zhu, Y., Xue, J., Wang, T., Song, T., Yang, Z., and Wang, S. (2018). The canonical E2Fs are required for germline development in Arabidopsis. Front. Plant Sci. **9:** 638.

Yelina, N.E., Smith, L.M., Jones, A.M., Patel, K., Kelly, K.A., and Baulcombe, D.C. (2010). Putative Arabidopsis THO/TREX mRNA export complex is involved in transgene and endogenous siRNA biosynthesis. Proc. Natl. Acad. Sci. USA **107:** 13948–13953.

Yoshikawa, M., Iki, T., Tsutsui, Y., Miyashita, K., Poethig, R.S., Habu, Y., and Ishikawa, M. (2013). 3′ fragment of miR173-programmed RISC-cleaved RNA is protected from degradation in a complex with RISC and SGS3. Proc. Natl. Acad. Sci. USA **110:** 4117–4122.

Yoshikawa, M., Peragine, A., Park, M.Y., and Poethig, R.S. (2005). A pathway for the biogenesis of trans-acting siRNAs in Arabidopsis. Genes Dev. **19:** 2164–2175.

Zhao, L., Cai, H., Su, Z., Wang, L., Huang, X., Zhang, M., Chen, P., Dai, X., Zhao, H., Palanivelu, R., Chen, X., and Qin, Y. (2018). *KLU* suppresses megasporocyte cell fate through SWR1-mediated activation of *WRKY28* expression in *Arabidopsis*. Proc. Natl. Acad. Sci. USA **115:** E526–E535.

Zheng, Y., Zhang, K., Guo, L., Liu, X., and Zhang, Z. (2018). AUXIN RESPONSE FACTOR3 plays distinct role during early flower development. Plant Signal. Behav. **13:** e1467690.